



SYNTHESIS AND CHARACTERIZATION OF TRANSITION METAL COMPLEX (CUO) NANOPARTICLES BY SOL-GEL METHOD

Vaibhav Namdev Gore^{1,3}, Ajit Hanumant Deshmukh², Gajanan Shankar
Rashinkar², Mohan Marthand Rajmane¹, Appasaheb Wamanrao
Suryawanshi^{3*}

¹Sadguru Gadage Maharaj College Karad-415124, Dist- Satara, M.S. India.

²Shivaji University Kolhapur, M.S. India.

³Department of Chemistry, Shri Madhavrao Patil Mahavidyalaya Murum, Tal-Omerga, Dist- Osmanabad-413605

* Corresponding author Email: sury44444@yahoo.com

Article History: Received: 18.04.2023

Revised: 04.05.2023

Accepted: 16.06.2023

Abstract: To create copper oxide (CuO) nanostructures with size- and shape-controlled morphologies, a base-catalyzed sol-gel method is supplemented with a solvent-driven self-assembly procedure at low temperature. CuO nanostructures have been created using very nanoporous thin sheets. The simulated XRD pattern of CuO nanostructures is consistent with the actual XRD patterns, and it indicates that the nanocrystal unit cell structure is monoclinic. The production and characterisation of nanoparticles with prospective applications are assessed in this study. Sol-gel method was used to create nanoscale Cu oxide particles. Transmission electron microscopy (TEM), Fourier transform infrared (FTIR) spectroscopy, X-ray diffraction (XRD), thermogravimetric analysis (TGA), specific surface area (SSA), and total chemical analysis were used to characterize nanoparticles (NPs). All of the synthesized NPs were in oxide form, and they were all examined for size, shape, surface structure, crystallinity, and elemental ratios. The findings show that all of the produced NPs were in their respective oxide forms of CuO and varied in size from 20 to 50 nm.

Keywords: Transition metal Oxides, sol-gel approach, nano particles.

DOI: 10.48047/ecb/2023.12.si7.519

INTRODUCTION

Green chemistry, also known as sustainable chemistry, is described by the Environmental Protection Agency as "the production of chemical products and processes which have the ability to reduce or eliminate the use or generation of hazardous substances." It has become increasingly predicted that chemists and chemical engineers will create chemical processes that are more environmentally friendly and long-lasting in the next decades.[1] Innovations in catalysis appear to be becoming increasingly important in the fields of energy, synthesis, and the environment since the world currently faces enormous problems relating to the atmosphere, energy, and environment. With the development of nanotechnology in recent years, the research on improved catalysts and catalytic activity has changed. [2]

One of the first applications of nanoparticles was in catalysis. In the past several decades, a variety of elements and substances, including aluminum, iron, titanium dioxide, and silica, have all been used as nanoscale catalysts [3, 4]. However, the proper explanation of the enormous synergist behavior that NPs exhibit despite everything has not been fully understood. Massive surface areas of nanoparticles have a clear positive effect on reaction rates and may also be a logical explanation for the reactant migration. At the nanoscale scale, any substance's qualities that depend on its structure and form can also affect how a material reacts. In terms of synthesis, shape, and size, the calibration of nano catalyst has produced noticeably higher selectivity. Thus, the question at hand is how nanoparticles' physical characteristics affect the properties of their reactants and how manufacturing boundaries might affect those characteristics [5]. A researcher may build and develop nano catalyst that are extremely dynamic, profoundly unique, and exceptionally tough by better understanding them. Each of these topics of interest

will enable contemporary synthetic reactions to become more resource efficient, use fewer resources, and generate less waste, which helps to mitigate the ecological impact caused by our reliance on the synthesis process. Nanoparticles are regarded as the most important contemporary catalyst and have a wider range of uses, including energy storage and transformation as well as chemical manufacture.[6] Selectivity and reactivity of the NPs have a fundamental significance as it can affect the course of a reaction that primarily depends on the surface area of NPs. The preparation of NPs in generally controlled size is primarily made by utilizing various stabilizing operators, such as ligands, surfactants, polymers, and so forth. Along these lines, control of surface structure and morphology and control of surface compositions are basically the two issues that determine the selectivity and reactivity of NPs. [7]. Recyclability of nanocatalyst continues to be a barrier to current NP usage. In contrast to other physical techniques like fluid extraction, chromatography, refining, filtration, or centrifugation, magnetic NPs has emerged as a powerful, exceptionally effective, and quick detachment material with many interesting points of comparison. Because of the strong interaction between magnetic nanoparticles and an externally applied magnetic field, the nanocatalyst immobilized on excessively paramagnetic nanomaterials can be effectively isolated from the objects and very well may be effectively dispersed once again in the absence of the magnetic field.[8] By thinking about how the distinctive qualities of nanoparticles affect catalytic activity, the idea behind nano catalysis may be understood. Nanomaterials' distinctive properties that significantly influence their synergistic action can be divided into four categories: (I) amounts that are directly related to bond length, such as the lattice parameter, density, and binding energy; (II) amounts that depend on the cohesive energy; (III) properties that differ with the density of binding energy; and (IV) properties from the combined impact of density of binding energy and atomic cohesive energy. [9] Important products were produced by combining these significant transformations with the most recent generation of nanocatalysts very successfully [10–12]. Accelerating a certain reaction pathway is crucial for the production of compounds of industrial relevance. Catalysts must be properly changed for enhanced selectivity since reaction selectivity is necessary for catalysis to promote the desired reactions. Utilizing nano-sized catalyst, which is presently the most efficient approach to further increase chemical processes, is one technique to improve the catalyst [13, 14]. These nanostructured materials have so far been used in many different kinds of organic transformations, such as chemo-selective oxidations, coupling reactions, hydrogen transfer processes, asymmetric hydrogenations, heterocyclic compounds, and more. Numerous catalytic applications have made use of a wide range of nanostructures, such as morphology-dependent nanocatalysts, graphene-supported nanocatalysts, and hybrid nanostructured catalysts.[15]

Nanostructures may have mesoporous structures as a result of the sol-gel technique, which involves the generation of seed crystals, their self-assembly, crystal development, and the production of void spaces between nanocrystals. As a result, these nanostructures' mesoporosity is also assessed. Manganese oxide and magnesium hydroxide nanostructures have extremely mesoporous surfaces with a sizably large surface area. In order to produce well-defined, extremely mesoporous nanostructures of copper oxide with high crystallinity, the sol-gel technique proposed and proven herein is used.

The sol-gel process is often carried out in a liquid state and at low temperatures (typically less than 100°C). The end product is solid, of course, and these solids are created during the polymerization process, which entails creating M-OH-M or M-O-M (where M stands for the metal atom) bonds between the metal atoms in the raw materials. The two processes that make up the sol-gel technique for synthesizing aerogels are as follows:(i) The production of distinct, colloidal solid particles of nanoscale diameters occurs in the first step. Colloidal particles in the solvent come together in the second stage to create a gel.

EXPERIMENTAL

Materials and reagents

Aryl aldehyde and 2- amino benzthiazole were procured from the Sigma-Aldrich chemicals. Ethanol (Reagent Alcohol, 140 Proof), toluene, magnesium(II)chloride hexahydrate, manganese(II)acetate

(anhydrous), and sodium hydroxide pellets were obtained from Fisher Scientific. Copper(II) acetate monohydrate was obtained from Alfa Aesar. All chemicals were used as received.

Preparation of TMO nanoparticles by Sol-gel method

In the sol-gel technique, condensation and polymerization processes take place after the hydrolysis of reactive metal precursors.

Produced from aryl aldehyde and 2-aminobenzthiazole, isatoic anhydride. Additionally, the isatoic anhydride interacts with CuO to generate TMO nanoparticles.

Metal oxides first go through hydrolysis, when the alkoxy group is changed to a hydroxo ligand. This process is also known as hydrolysis or ligand exchange. Alcohol or water is then removed after condensation to create metal oxide or hydroxide connections. Only when the cation metal is linked to at least one hydroxo ligand—referred to as Metal-OH for convenience—does condensation take place. 250 mL round bottom flasks with an oil bath and ambient air were used for the reactions. Deionized H₂O, 70% EtOH, DMF, and toluene were the four distinct solvents used to create each metal oxide nanomaterial. For each nanomaterial, a metal precursor was created using one of the following: 1.2 g of copper acetate. A solvent (200 mL) was introduced to the flask in a normal technique. In 10 mL of deionized water, a metal precursor was dissolved before being introduced to the reaction flask. The reaction flask was then agitated for an additional 5 minutes while sodium hydroxide (NaOH) pellets were dissolved in deionized water (10 mL) and added dropwise at a rate of 10.0 mL min⁻¹. The flask was placed in a non-heated oil bath at room temperature after stirring for 5 min. at room temperature. To avoid bumping, hot stones were poured to the flask before heating the bath. Following a 24 hour wait, the flask was progressively heated to 80°C. The reaction flask was then allowed to cool over the course of several hours to room temperature. After transferring the colloidal solution into centrifuge tubes, the liquid was spun at 1000 rpm for 10 minutes, the liquid was decanted, and the product was then rinsed with de-ionized water. SEM, TEM, and XRD analysis were performed on the dried powder.

Table 1: Experimental conditions and morphologies of respective CuO nanostructures

Molar ratio	Solvent type/water	Morphology (dimension/nm)
1 : 5	Water	110
	ethanol	118
	DMF	48
	Toluene	138
1 : 10	Water	112
	ethanol	120
	DMF	49
	Toluene	133
1 : 15	Water	109
	ethanol	123
	DMF	51
	Toluene	134

Synthetic scheme

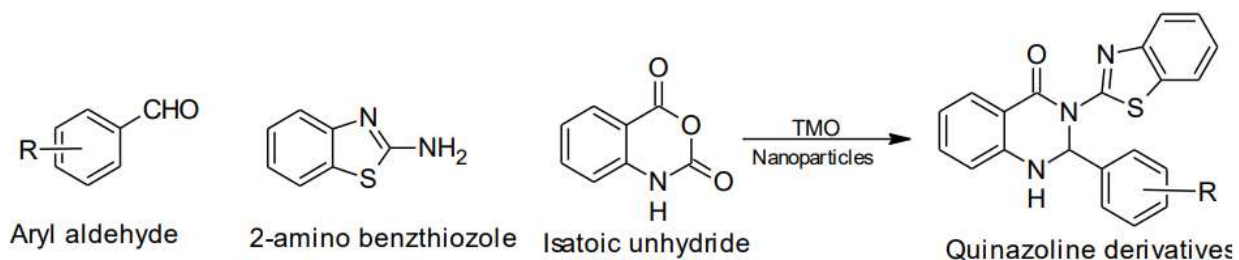


Figure 1: Synthesis of TMO nanoparticles.

Identification of Intermediate I by TLC

Intermediate I and final product was identified after synthesis by performing TLC. The TLC showed 2 different spots, which confirms the synthesis of Intermediate I and Final product.

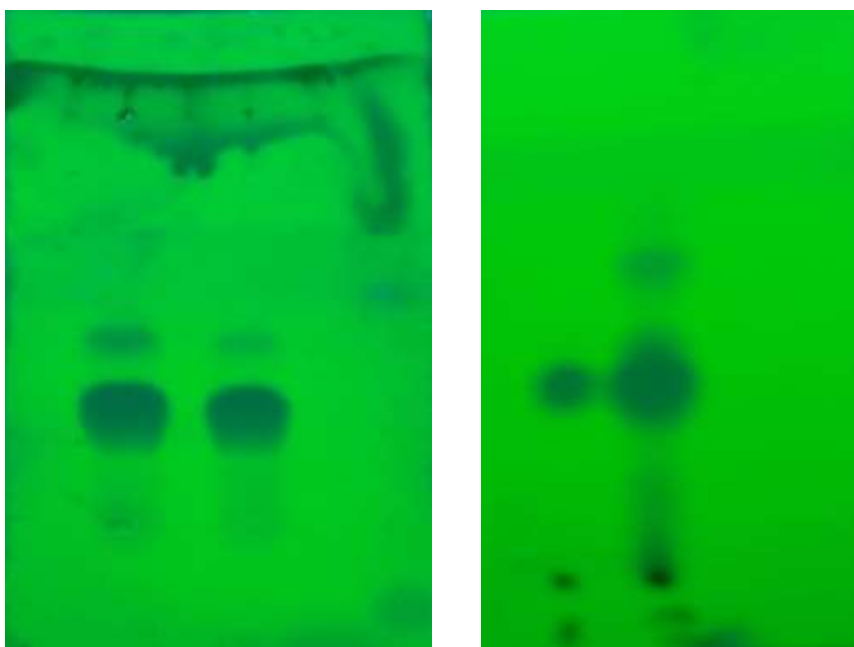
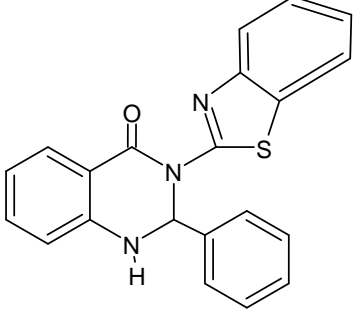


Figure 1: TLC spot of a) Intermediate I b) Final Product

Chemical Structure	IUPAC name	Molecular Formula	Molecular Weight	% Yield	Melting Point
	2H-3,1-benzoxazine-2,4(1H)-dione	$C_8H_5NO_3$	163.13	45	218

 <p>Intermediate II</p>	<p>3-(1,3-benzothiazol-2-yl)-2-phenyl-2,3-dihydroquinazolin-4(1H)-one</p>	<p>C₂₁H₁₅N₃O₂S</p>	<p>357.42</p>	<p>53</p>	<p>219</p>
-----------------------------------------------------------------------------------------------------------------	---------------------------------------------------------------------------	-----------------------------------------------------------------------	----------------------	------------------	-------------------

**¹H NMR
Characterization**

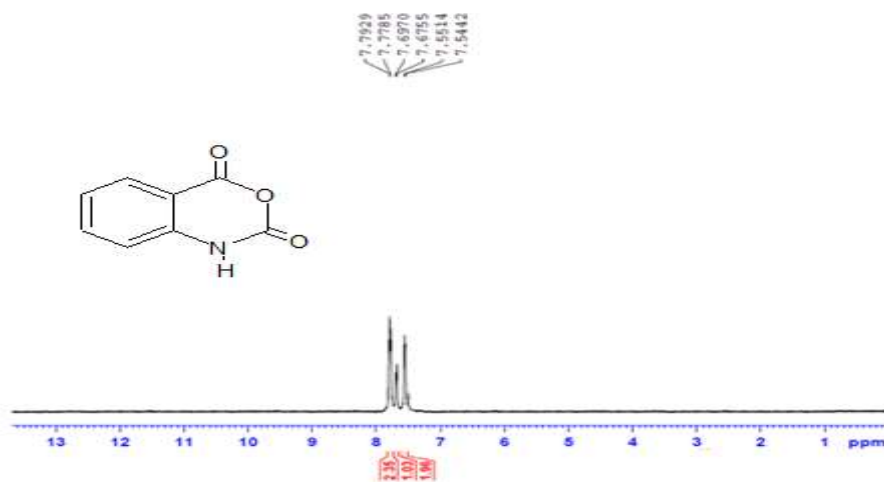


Figure 2: ¹H NMR spectra of 2H-3,1-benzoxazine-2,4(1H)-dione

¹H NMR: δ 7.31-7.47 (2H, 7.38 (ddd, J = 8.1, 1.4, 0.5 Hz), 7.40 (ddd, J = 7.9, 7.5, 1.4 Hz)), 7.70 (1H, ddd, J = 8.1, 7.5, 1.5 Hz), 7.92 (1H, ddd, J = 7.9, 1.5, 0.5 Hz).

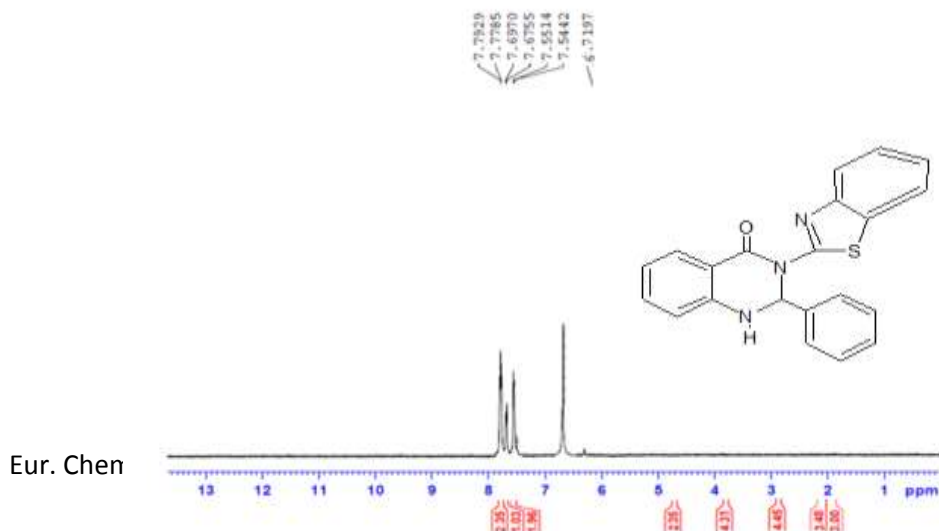


Figure 3: 3-(1,3-benzothiazol-2-yl)-2-phenyl-2,3-dihydroquinazolin-4(1H)-one

$^1\text{H NMR}$: δ 6.22 (1H, s), 6.96 (1H, ddd, $J = 8.1, 1.2, 0.5$ Hz), 7.13-7.71 (11H, 7.19 (dtd, $J = 8.0, 1.3, 0.5$ Hz), 7.25 (ddd, $J = 8.0, 6.9, 1.3$ Hz), 7.31 (ddd, $J = 7.9, 7.4, 1.2$ Hz), 7.35 (tt, $J = 7.5, 1.3$ Hz), 7.37 (ddd, $J = 7.9, 6.9, 1.4$ Hz), 7.49 (dddd, $J = 8.0, 7.5, 1.6, 0.5$ Hz), 7.58 (ddd, $J = 7.9, 1.4, 0.5$ Hz), 7.62 (ddd, $J = 8.1, 7.4, 1.4$ Hz), 7.64 (ddd, $J = 7.9, 1.3, 0.5$ Hz), 7.79 (1H, ddd, $J = 8.0, 1.4, 0.5$ Hz).

LCMS

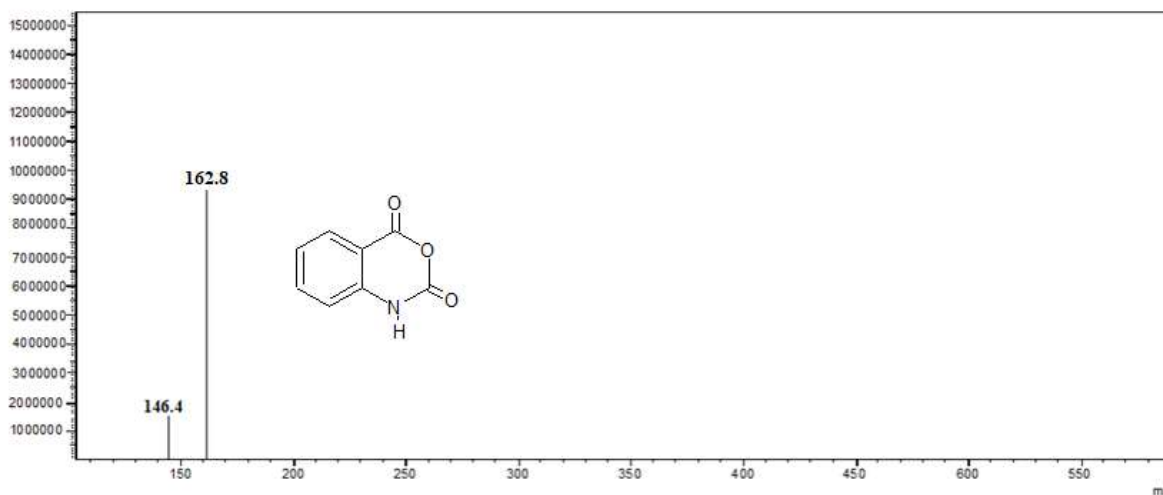


Figure 4: MASS spectra of 2H-3,1-benzoxazine-2,4(1H)-dione

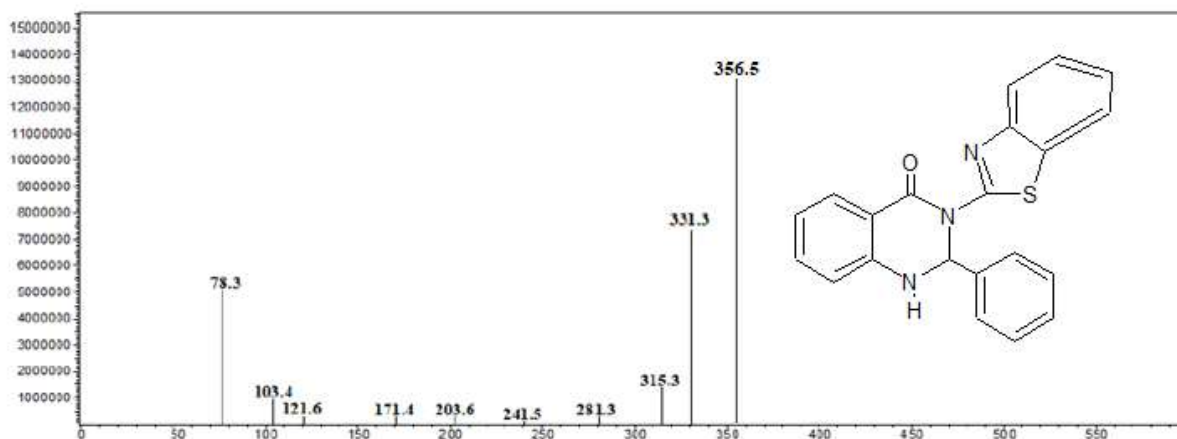


Figure 5: Mass spectra of 3-(1,3-benzothiazol-2-yl)-2-phenyl-2,3-dihydroquinazolin-4(1H)-one

XRD

A crystalline material's phase was identified via X-ray diffraction. X-rays need a lot of energy to enter a substance, and their wavelengths are on par with the spacing between atoms in materials. The XRD patterns were captured using a nickel-filtered CuK radiation source (0.15418 nm) and a scintillation

counter detector on a BRUKER AXS (Model: D8 FOCUS) instrument. By measuring the angles at which an X-ray is diffracted by the sample, powder diffraction profiles may be derived (Bragg's Law) [11]. The intensity data were collected over a 2θ range of 10- 80°. The crystallite size were determined by using Scherrer equation as mentioned below-

$D = K \lambda / \beta \cos \theta$ (1) Where λ is the wavelength of X-ray source ($\text{CuK}\alpha = 0.15418 \text{ nm}$), β is the full width at half maximum (FWHM), θ is the diffraction angle, K is shape factor, D is mean size of the ordered (crystalline) domain.

SEM

The surface of the sample is imaged by the SEM, a type of electron microscope, by scanning it with a high-energy electron beam in a raster scan pattern. SEM analyses were carried out to analyze the surface topology using "JEOL, JSM Model 6390 LV" scanning electron microscopes that operate at a 15 kV accelerating voltage. At the surface of solid objects, the SEM produces a variety of signals using a concentrated beam of high-energy electrons [16, 17]. In addition to the sample's exterior morphology (texture), chemical composition, and crystalline structure and orientation of its constituent components, the signals resulting from electron-sample interactions also provide information about the sample.

TEM

By accelerating an electron beam that travels through the specimen, the TEM creates a picture. In TEM, electrons are accelerated to 100 KeV or more (up to 1 MeV), projected onto a thin specimen (less than 200 nm), and either penetrate the sample thickness undeflected or deflected by means of the condenser lens system. Images may be used to learn about the size, shape, and distribution of particles in the support and active phases as well as how they relate to one another. With the use of an objective aperture and axial illumination, the high-resolution transmission electron microscopy (HRTEM) approach combines a number of diffracted beams with the axial transmitted beam to create the picture [19, 20]. The TECNAI G2 20 S-TWIN (FEI COMPANY, USA) with a resolution of 2.4, fitted with a slow scan CCD camera and an accelerating voltage of 200 kV, was used in this work to conduct the electron microscopy examinations.

RESULT & DISCUSSION

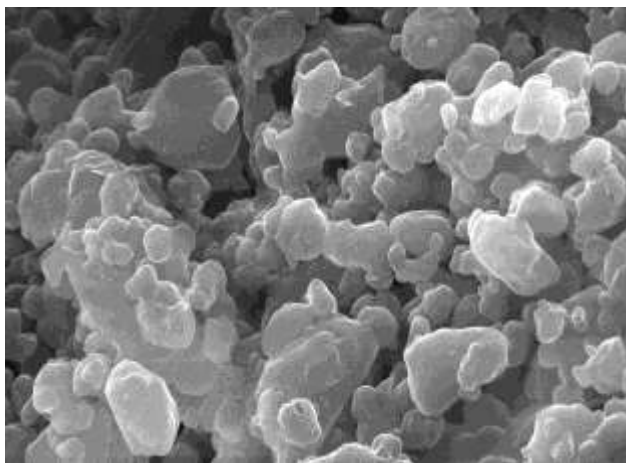
After the samples were cleaned and redistributed in de-ionized water, the morphologies of the nanostructures were examined using SEM and TEM. CuO nanostructures with shape-controlled morphologies were produced in relation to water and three distinct solvent systems, as shown in Table. The SEM investigation of the final products produced by various solvent systems reveals two unique morphologies: aggregated irregularly shaped nanoparticles for optimal reactivity and hexagonal nanoparticles.

Water, ethanol, and toluene produced hexagonal nanoparticles with an average diameter of 100 nm to 200 nm. The reaction tends to produce aggregated nanoparticles that are confined in gel-like formations, despite the fact that hexagonal nanoparticles produced in water at a 15 molar ratio. Comparatively to the hexagonal nanoparticles created at all other solvent systems and molar ratios, the hexagonal nanoparticles formed at a 10 molar ratio of the precursor to the base in a water/toluene solvent combination have well-defined edges with a very uniform size distribution. This may be caused by toluene's relatively poor water miscibility, which results in a large concentration of toluene molecules that are not solvated. In contrast to the particles produced in water and water/ethanol systems, it was able to regulate the development of the nanocrystals along the facets by acting as shape-controlling toluene molecules. This resulted in well-defined hexagonal nanoparticles. However, in general, for all three distinct base concentrations, nanostructures produced in all four solvent systems have a larger size variety, but the particle size tends to decrease as the base concentration increases. For instance, hexagonal nanoparticles made in water demonstrate that the diameter reduces as the base concentration rises. Particle diameter is around 200 nm

at 15 molar ratio, but at 15 molar ratio, the average diameter was lowered to about 100 nm. The fact that the average diameter of the particles created in ethanol did not noticeably rise—retaining its average diameter at or around 150 nm—indicates that, despite an increase in base concentration, particle size was kept within a limited size distribution. We think that the nucleation rate maximum at a certain base concentration, in our example at 15 molar ratio, and is independent at higher base concentrations, therefore this may be caused by a larger base solvation in water/ethanol, generating a homogenous solution. Because solvent molecules act as surfactants to control crystal growth, the size distribution of seed crystals may be homogeneous at all three base concentrations while their growth is controlled by the surface energies of their facets. As a result, size-controlled nanostructures are produced at all three base concentrations.

SEM

The SEM investigation of the final products produced by various solvent systems reveals two unique morphologies: aggregated irregularly shaped nanoparticles and hexagonal nanoparticles. In water, ethanol, and toluene, hexagonal nanoparticles with an average diameter of 50 nm to 150 nm were



produced.

Figure 6: SEM graph of optimized batch

TEM

The TEM images further reveals the particles shape and size, confirming the hexagonal shape for nanoparticles formed in water, ethanol, and toluene.

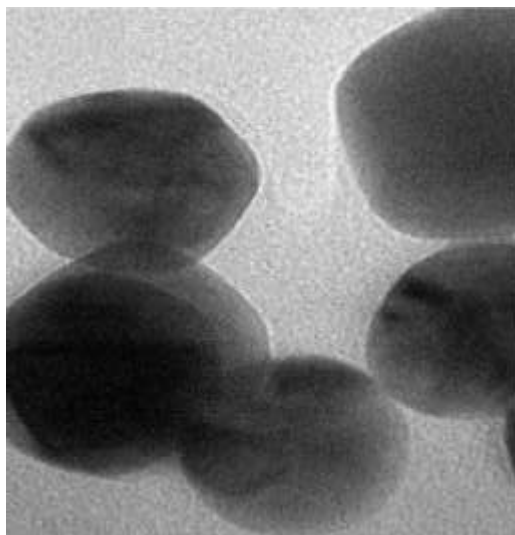


Figure 7: TEM graph of optimized batch

XRD

XRD Additionally, it was evident that the CuO XRD reflections matched the monoclinic structure. According to the figure, the planed copper oxide NPs are responsible for the diffraction peaks, which is in good accord with previous published results.

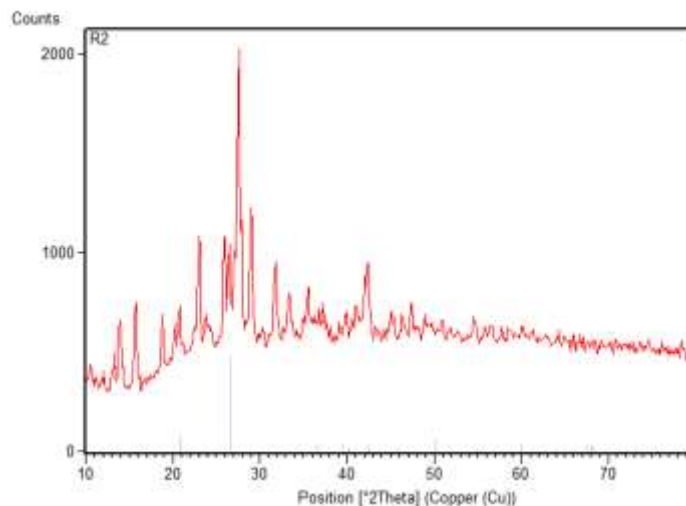


Figure 8: XRD graph pf optimized batch

CONCLUSION

In conclusion, the production of copper oxide (CuO) nanoparticles using the sol-gel technique has been simplified into a single step. The repeatability of the finished result in order to prevent other concerns generated by other procedures is a key advantage of this method over other methods. To confirm the structure, ¹HNMR and MASS were used to describe intermediates I and II (the final product). Transmission electron microscopy (TEM), Fourier transform infrared (FTIR) spectroscopy, X-ray diffraction (XRD), thermogravimetric analysis (TGA), specific surface area (SSA), and total chemical analysis were used to characterize nanoparticles (NPs). All of the synthesized NPs were in oxide form, and they were all examined for size, shape, surface structure, crystallinity, and elemental ratios. The findings show that all of the produced NPs were in their respective oxide forms of CuO and varied in size from 20 to 50 nm.

CONFLICT OF INTEREST

None declare by authors.

REFERENCES

1. Dunn PJ. The importance of green chemistry in process research and development. *Chemical Society Reviews*. 2012;41:1452-1461
2. J.A. Darr, J. Zhang, N.M. Makwana, X. Weng, Continuous hydrothermal synthesis of inorganic nanoparticles: applications and future directions, *Chemical reviews*, 117 (2017) 11125-11238.
3. Y. Guo, Z. Wang, H. Shao, X. Jiang, Hydrothermal synthesis of highly fluorescent carbon nanoparticles from sodium citrate and their use for the detection of mercury ions, *Carbon*, 52 (2013) 583-589.

4. M. Zhu, Y. Wang, D. Meng, X. Qin, G. Diao, Hydrothermal synthesis of hematite nanoparticles and their electrochemical properties, *The Journal of Physical Chemistry C*, 116 (2012) 16276- 16285.
5. A.K. Ganguli, T. Ahmad, S. Vaidya, J. Ahmed, Microemulsion route to the synthesis of nanoparticles, *Pure and Applied Chemistry*, 80 (2008) 2451-2477.
6. M. López-Quintela, J. Rivas, M. Blanco, C. Tojo, Synthesis of nanoparticles in microemulsions, in: *Nanoscale materials*, Springer, 2004, pp. 135-155.
7. S.R. Patade, D.D. Andhare, S.B. Somvanshi, S.A. Jadhav, M.V. Khedkar, K. Jadhav, Selfheating evaluation of superparamagnetic MnFe₂O₄ nanoparticles for magnetic fluid hyperthermia application towards cancer treatment, *Ceramics International*, (2020).
8. P.B. Kharat, S. More, S.B. Somvanshi, K. Jadhav, Exploration of thermoacoustics behavior of water based nickel ferrite nanofluids by ultrasonic velocity method, *Journal of Materials Science: Materials in Electronics*, 30 (2019) 6564-6574.
9. S.B. Somvanshi, R.V. Kumar, J.S. Kounsalye, T.S. Saraf, K. Jadhav, Investigations of structural, magnetic and induction heating properties of surface functionalized zinc ferrite nanoparticles for hyperthermia applications, in: *AIP Conference Proceedings*, AIP Publishing LLC, 2019, pp. 030522.
10. A.R. Chavan, S.B. Somvanshi, P.P. Khirade, K. Jadhav, Influence of trivalent Cr ion substitution on the physicochemical, optical, electrical, and dielectric properties of sprayed NiFe₂O₄ spinel-magnetic thin films, *RSC Advances*, 10 (2020) 25143-25154.
11. H. Kardile, S.B. Somvanshi, A.R. Chavan, A. Pandit, K. Jadhav, Effect of Cd²⁺ doping on structural, morphological, optical, magnetic and wettability properties of nickel ferrite thin films, *Optik*, (2020) 164462.
12. G. Kulkarni, P.J. Thomas, C. Rao, Mesoscopic assembly and other properties of metal and semiconductor nanocrystals, *The Chemistry of Nanomaterials: Synthesis, Properties and Applications*, (2004) 51-93.
13. W. Niu, G. Xu, Crystallographic control of noble metal nanocrystals, *Nano Today*, 6 (2011) 265-285.
14. S. Sadjadi, M.H. Majid, M. Malmir, Pd (0) nanoparticle immobilized on cyclodextrinanosponge-decorated Fe₂O₃@ SiO₂ core-shell hollow sphere: an efficient catalyst for CC coupling reactions, *Journal of the Taiwan Institute of Chemical Engineers*, 86 (2018) 240-251.
15. S.L. Candelaria, Y. Shao, W. Zhou, X. Li, J. Xiao, J.-G. Zhang, Y. Wang, J. Liu, J. Li, G. Cao, Nanostructured carbon for energy storage and conversion, *Nano energy*, 1 (2012) 195-220.